Cancer Immunology, Immunotherapy (2025) 74:137
https://doi.org/10.1007/s00262-025-03994-5

RESEARCH

Clofazimine enhances anti-PD-1 immunotherapy in glioblastoma by inhibiting Wnt6 signaling and modulating the tumor immune microenvironment

Yuze Zhao[1] · Yuguang Song[3] · Weiping Li[4] · Jiangping Wu[5] · Zhengbao Zhao[6] · Tingli Qu[6] · Hong Xiao[7] · Manyuan Wang[8] · Min Zhu[9] · Peiming Zheng[7] · Huili Wan[7] · Qingkun Song[5] · Huixia Zheng[7] · Shuo Wang[2]

Received: 18 January 2025 / Accepted: 21 February 2025 / Published online: 7 March 2025

Abstract

Glioblastoma multiforme (GBM) is an aggressive and lethal primary brain tumor with limitedtreatment options due to its resistance to conventional therapies and an immunosuppressive tumor microenvironment. In this study, we investigated whether clofazimine, an inhibitor of the Wnt/β-catenin signaling pathway, could enhance the efficacy of anti-PD-1 immunotherapy in GBM. Our in vitro and in vivo experiments demonstrated that clofazimine suppressed GBM cell proliferation, induced apoptosis, and inhibited invasion by downregulating Wnt6-mediated activation of the Wnt/β-catenin pathway and the downstream MEK/ERK signaling cascade, leading to decreased PD-L1 expression. Notably, the combination of clofazimine and anti-PD-1 therapy significantly reduced tumor growth and intracranial invasion in orthotopic GBM mouse models, resulting in extended survival. This combination therapy also reshaped the tumor immune microenvironment by increasing cytotoxic $CD8^+$ T cell infiltration, reducing regulatory T cells, and promoting T cell receptor clonality and diversity, indicative of a robust anti-tumor immune response. Our findings suggest that clofazimine enhances the therapeutic effects of anti-PD-1 immunotherapy in GBM through modulation of the Wnt6/β-catenin/PD-L1 axis and reshaping the immune microenvironment. While these results are promising, further clinical studies are needed to evaluate the efficacy and safety of this combinatory approach in GBM patients.

Keywords Clofazimine · Anti-PD-1 immunotherapy · Glioblastoma · Wnt6 signaling pathway · Tumor immune microenvironment

Yuze Zhao, Yuguang Song, Weiping Li, and Shuo Wang have contributed equally to this article.

✉ Qingkun Song
songqingkun@ccmu.edu.cn

✉ Huixia Zheng
huixiazheng62@126.com

✉ Shuo Wang
wangshuo919@163.com

[1] Department of Medical Oncology, Capital Medical University Cancer Center, Beijing Shijitan Hospital, Capital Medical University, Beijing 100038, China

[2] Department of Medical Oncology, Beijing Youan Hospital, Capital Medical University, Beijing 100069, China

[3] Department of Radiotherapy, Capital Medical University Cancer Center, Beijing Shijitan Hospital, Capital Medical University, Beijing 100038, China

[4] Department of Pharmacology, Shanxi Medical University Fenyang College, Fenyang 032200, China

[5] Department of Center of Biobank, Beijing Youan Hospital, Capital Medical University, Beijing 100069, China

[6] Department of Pharmacy, Shanxi Medical University, Taiyuan 030001, China

[7] Department of Pathology, First Hospital of Shanxi Medical University, Taiyuan 030001, China

[8] Beijing Key Laboratory of TCM Collateral Disease Theory Research, School of Traditional Chinese Medicine, Capital Medical University, Beijing 100069, China

[9] State Key Laboratory of Cardiovascular Disease, National Center for Cardiovascular Diseases, Fuwai Hospital, Key Laboratory of Application of Pluripotent Stem Cells in Heart Regeneration, Chinese Academy of Medical Sciences and Peking Union Medical College, Beijing, China

Introduction

Glioblastoma multiforme (GBM) is the most aggressive and fatal primary brain tumor in adults, accounting for approximately 48% of all malignant central nervous system tumors worldwide [1–3]. Despite advances in neurosurgery, radiotherapy, and chemotherapy, the median overall survival of patients with GBM remains around 15 months, and the five-year survival rate is less than 10% [3]. The poor prognosis is attributed to the highly invasive nature of GBM cells, significant intratumoral heterogeneity, and the presence of an immunosuppressive tumor microenvironment (TME) that hinders effective therapeutic interventions [4, 5].

Immunotherapy, particularly immune checkpoint inhibitors (ICIs) targeting programmed death receptor-1 (PD-1) and its ligand PD-L1, has transformed the treatment landscape of several solid tumors, including melanoma and non-small cell lung cancer [6, 7]. However, in GBM, clinical trials of anti-PD-1 monotherapy have not demonstrated significant therapeutic benefits [8, 9]. This lack of efficacy is due to several factors: the immunosuppressive TME characterized by the accumulation of regulatory T cells (Tregs), myeloid-derived suppressor cells (MDSCs), and M2-polarized tumor-associated macrophages (TAMs); the low mutational burden and paucity of neoantigens in GBM cells leading to poor immunogenicity; and the presence of the blood–brain barrier (BBB), which restricts the penetration of immune cells and therapeutic agents into the tumor site [10].

Given these challenges, there is an urgent need to develop novel therapeutic strategies that can enhance the efficacy of ICIs in GBM. One promising approach is to combine ICIs with agents that can modulate the TME, inhibit tumor-intrinsic pathways contributing to immune evasion, and promote immune cell infiltration [11]. The Wnt/β-catenin signaling pathway has emerged as a critical mediator of tumor progression and immune resistance in GBM [12, 13]. Aberrant activation of this pathway is associated with increased proliferation, invasion, stemness, and resistance to apoptosis in GBM cells [14, 15]. Moreover, Wnt/β-catenin signaling contributes to the immunosuppressive TME by inhibiting dendritic cell maturation, reducing T cell infiltration, and upregulating immune checkpoint molecules such as PD-L1 on tumor cells [16].

Clofazimine, an FDA-approved riminophenazine antibiotic traditionally used for the treatment of leprosy, has recently gained attention for its anti-cancer properties [17]. Studies have shown that clofazimine can inhibit the Wnt/β-catenin signaling pathway, leading to suppressed tumor growth in various cancer models [17]. In GBM, targeting Wnt signaling offers the potential to not only inhibit tumor cell proliferation and invasion but also to modulate the TME towards a more immunostimulatory state [12] The Wnt pathway, particularly WNT6, plays a crucial role in the development of glioblastoma (GBM). WNT6 is highly expressed in some gliomas, independent of IDH mutations and 1p/19q co-deletion status. Its expression is regulated by DNA methylation in both the promoter and gene body. PLAGL2, an oncogene in gliomas, upregulates WNT6 and other Wnt signaling elements, promoting GBM stem cell maintenance and tumor progression. Additionally, HOXA9 has been identified as a key transcriptional regulator of WNT6, activating the WNT/β-catenin pathway in GBM. Clinically, high WNT6 expression correlates with poor prognosis in GBM patients, making it an independent prognostic biomarker [18, 19].

In this study, we investigated the effects of clofazimine on GBM cells both in vitro and in vivo. We demonstrated that clofazimine effectively downregulated Wnt6 expression and inhibited the Wnt/β-catenin signaling cascade, leading to decreased PD-L1 expression and suppression of epithelial-mesenchymal transition (EMT) markers. In an orthotopic GBM mouse model, the combination of clofazimine and anti-PD-1 therapy significantly reduced tumor growth, decreased intracranial invasion, and prolonged survival compared to monotherapy or control groups. Importantly, clofazimine modulated the TME by increasing the infiltration of cytotoxic $CD8^+$ T cells, reducing the population of Tregs, and altering the macrophage polarization towards a pro-inflammatory phenotype. Our findings suggest that clofazimine enhances the anti-tumor efficacy of anti-PD-1 immunotherapy in GBM by targeting both tumor-intrinsic Wnt6 signaling and the immunosuppressive TME. This combinatorial approach holds promise as a novel therapeutic strategy to overcome immune resistance in GBM and improve patient outcomes.

Results

Clofazimine enhances the therapeutic effects of anti-PD-1 immunotherapy in inhibiting glioblastoma growth and intracranial invasion in vivo

To assess the in vivo efficacy of clofazimine in enhancing anti-PD-1 treatment for glioblastoma (GBM), we utilized orthotopic GBM mouse models (Fig. 1A). GL261 cells were implanted into the brains of C57BL/6 mice, which were subsequently divided into four treatment groups: control, clofazimine monotherapy, anti-PD-1 monotherapy, and combination therapy with clofazimine and anti-PD-1. Fluorescence imaging revealed that both clofazimine and anti-PD-1 monotherapies significantly reduced tumor fluorescence intensity

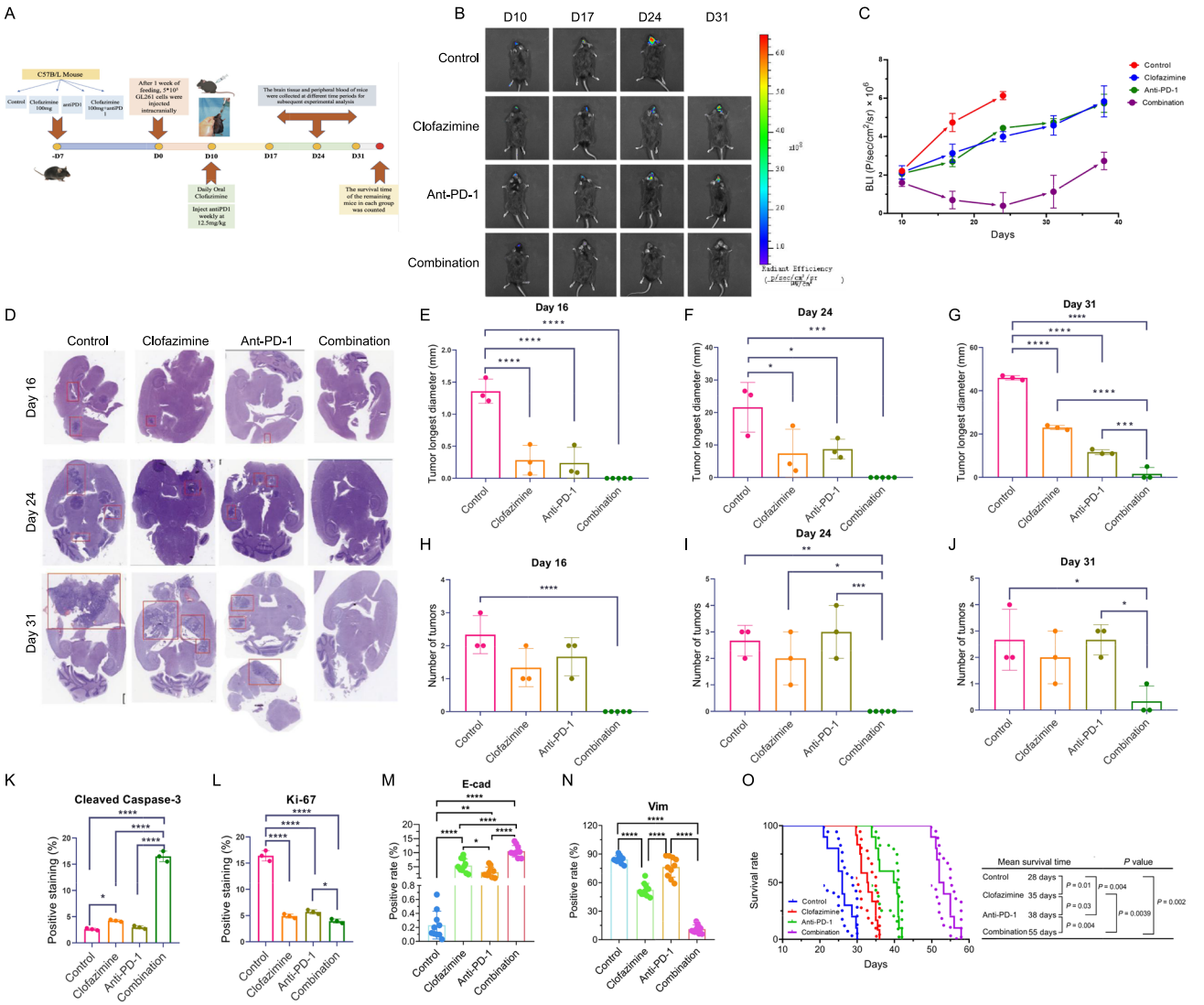

Fig. 1 Clofazimine enhances the therapeutic effects of anti-PD-1 immunotherapy in orthotopic glioblastoma mouse models. **A** Schematic representation of the experimental setup. GL261 cells were implanted into the brains of C57BL/6 mice, which were subsequently divided into four treatment groups: control, clofazimine monotherapy, anti-PD-1 monotherapy, and combination therapy with clofazimine and anti-PD-1. **B**, **C** In vivo bioluminescence imaging showing tumor growth in mice over time. The combination therapy group exhibited a sustained reduction in intracranial tumor volume compared to control and monotherapy groups. **D**–**G** Representative H&E staining of mouse brain sections showing tumor lesions. The combination therapy group had smaller tumor lesions. **H**–**J** Quantification of tumor lesions in different groups. The combination therapy group had a notable decrease in the number of tumor lesions. **K**, **L** Immunostaining for cleaved caspase-3 (**K**) and Ki-67 (**L**) in tumor sections. The combination therapy significantly induced apoptosis and reduced tumor cell proliferation. **M**, **N** Immunostaining for Vimentin (**M**) and E-cadherin (**N**). The combination therapy decreased Vimentin expression and increased E-cadherin expression, suggesting inhibition of EMT. **O** Kaplan-Meier survival curve showing prolonged survival in the combination therapy group compared to control and monotherapy groups.

compared to the control group (Fig. 1B and C). Importantly, the combination therapy exhibited a sustained reduction in intracranial tumor volume, surpassing the effects observed in the monotherapy groups (Fig. 1B and C).

Histological analysis further corroborated these findings, showing smaller tumor lesions in the combination therapy group (Fig. 1D–G), indicating effective repression of GBM growth. Additionally, there was a notable decrease in the number of tumor lesions in the combination therapy group compared to both control and monotherapy groups (Fig. 1H–J), suggesting that this treatment strategy effectively inhibits GBM intracranial invasion.

To further investigate the mechanisms underlying these effects, we evaluated the expression of proliferation-associated markers. Our data demonstrated that the combination therapy significantly induced apoptosis in GBM cells, as

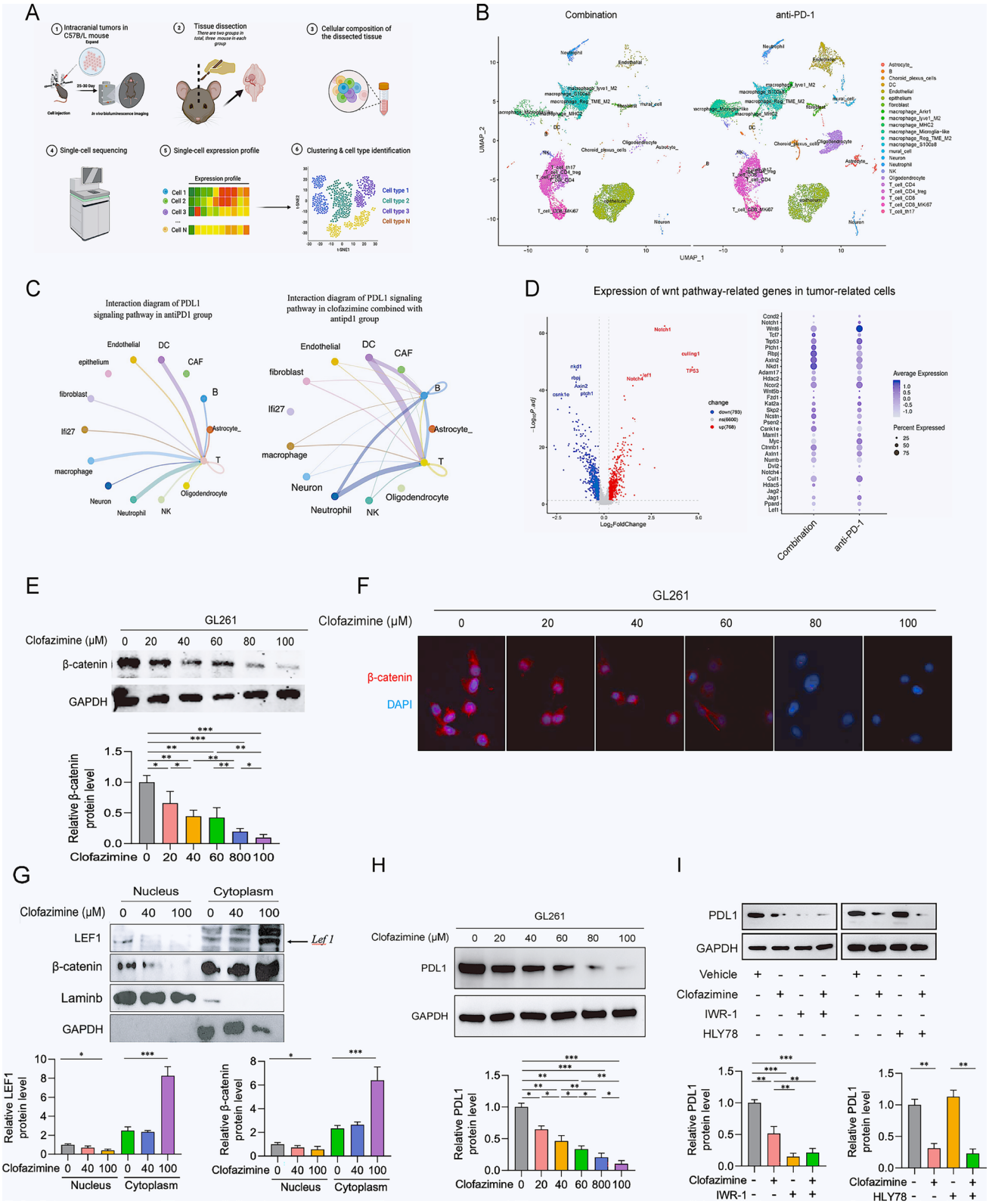

evidenced by increased levels of cleaved caspase-3 (Fig. 1K, Supplementary Fig. 1A). Conversely, Ki-67 staining indicated a marked reduction in tumor cell proliferation within the combination therapy group (Fig. 1L, Supplementary Fig. 1B). Furthermore, we examined the expression of epithelial-mesenchymal transition (EMT)-related markers,

◂**Fig. 2** Clofazimine decreases PD-L1 expression by inhibiting the Wnt/β-catenin pathway in GBM cells. **A**, **B** Single-cell RNA sequencing analysis of tumor tissues from orthotopic GBM mouse models. **C** The addition of clofazimine can effectively increase the crosstalk between PDL1. **D** The most prominently differentially expressed genes in the wnt pathway between the two groups. **E–F** Western blot and immunofluorescence analysis of β-catenin expression in GL261 cells. **G** Western blot analysis of β-catenin nuclear translocation in GBM cell lines treated with clofazimine. Clofazimine inhibited nuclear β-catenin in a dose-dependent manner. **H** Western blot and immunofluorescence analysis of PD-L1 expression in GL261 cells. **I** Western blot analysis showing that IWR-1 blocked the clofazimine-mediated decrease in PD-L1 expression, while HLY78 reversed this effect

revealing that the combination therapy effectively reduced the expression of mesenchymal marker, Vimentin, while increasing the expression of the epithelial marker E-cadherin (Fig. 1M and N, Supplementary Fig. 1C and D). This suggests that clofazimine, in conjunction with anti-PD-1, can inhibit the EMT phenomenon, thereby suppressing tumor invasion.

Importantly, the median overall survival of mice in the combination therapy group was significantly prolonged compared to the control and monotherapy groups, reaching 55 days (Fig. 1O). Collectively, these results indicate that clofazimine enhances the therapeutic effects of anti-PD-1 immunotherapy by effectively inhibiting GBM growth and invasion, ultimately leading to improved survival outcomes in orthotopic GBM mouse models.

Clofazimine decreases PD-L1 expression by inhibiting the Wnt/β-catenin pathway in GBM cells

To elucidate the mechanism by which clofazimine enhances the therapeutic efficacy of anti-PD-1 immunotherapy, we conducted single-cell sequencing analysis on tumor tissues obtained from orthotopic GBM mouse models (Fig. 2A and B). Our research delved deeply into the correlations of PD-L1 transcription among T cells, B cells, and other cell populations. Through comprehensive intercellular communication analysis, we found that T cells had direct and robust communication with various other cell subtypes. Moreover, the PD-L1 signaling pathways were identified as crucial mediators of intercellular communication in both two therapy groups. Particularly, in the combination group, our findings revealed a significantly higher number and stronger intensity of cell—cell communication interactions within the PD-L1 signaling pathway. Among these, the enhanced interaction between T cells and DC cells was an especially prominent discovery, which may have important implications for understanding the underlying mechanisms of the combined treatment (Fig. 2C). Additionally, we performed differential statistics on Wnt6-related genes in the two groups of mice, as shown in Fig. 2D. We found that the addition of clofazimine effectively inhibited Notch4, Notch1, Lef1 [20], and culling 1 expression, as promoters in Wnt6 signaling pathway, while increasing the key inhibitors, cxnk1e [21], ptch1 [22], Axin2 [23], Rbpj [24], and nkd1 [25].

To further investigate the impact of clofazimine on PD-L1 expression and the Wnt/β-catenin pathway, we treated GBM cell lines with clofazimine and performed western blot and immunofluorescence analyses. These analyses demonstrated that clofazimine inhibited the nuclear levels of β-catenin in a dose-dependent manner, indicating effective disruption of the Wnt/β-catenin pathway (Fig. 2E–G). Notably, this inactivation was accompanied by a significant decrease in PD-L1 expression (Fig. 2H).

To confirm that clofazimine reduces PD-L1 expression through the inactivation of the Wnt/β-catenin pathway, we utilized IWR-1, a specific inhibitor of this pathway, in our experiments. After the addition of IWR-1, which already inhibits the Wnt pathway, there is no significant decrease in PD-L1 expression with the subsequent treatment of clofazimine. This indicates that clofazimine primarily reduces PD-L1 expression by inhibiting the Wnt pathway. Conversely, clofazimine effectively inhibited the increase in PD-L1 expression induced by HLY78, an activator of the Wnt/β-catenin pathway (Fig. 2I). Collectively, these findings suggest that clofazimine inhibits the nuclear translocation of β-catenin and LEF-1, thereby inactivating the Wnt/β-catenin pathway and resulting in reduced PD-L1 expression in GBM cells.

Clofazimine inactivates the Wnt/β-catenin signaling by inhibiting Wnt6 expression in GBM cells

To further elucidate the mechanism by which clofazimine inactivates the Wnt/β-catenin signaling pathway, we re-analyzed the single-cell sequencing data. Our findings revealed that Wnt6 expression was significantly downregulated in the combination therapy group compared to the anti-PD-1 monotherapy group in GBM cells (Supplementary Fig. 2). This led us to hypothesize that clofazimine may suppress Wnt6 expression to inactivate the Wnt/β-catenin pathway.

To confirm this hypothesis, we examined the effects of clofazimine on Wnt6 expression in both human and mouse GBM cell lines, as well as on the expression of other Wnt ligands, including Wnt3a and Wnt4. Western blot analyses indicated that Wnt6 was the most sensitive to clofazimine treatment among the three Wnt ligands tested, exhibiting significant inhibition across all cell lines, while Wnt3a and Wnt4 showed only moderate sensitivity (Fig. 3A).

To further validate the regulatory role of Wnt6 in the Wnt/β-catenin pathway, we utilized siRNAs to knock down Wnt6 expression and the pcDNA3.1 vector to overexpress Wnt6 in GBM cells (Supplementary Fig. 3). Western blot

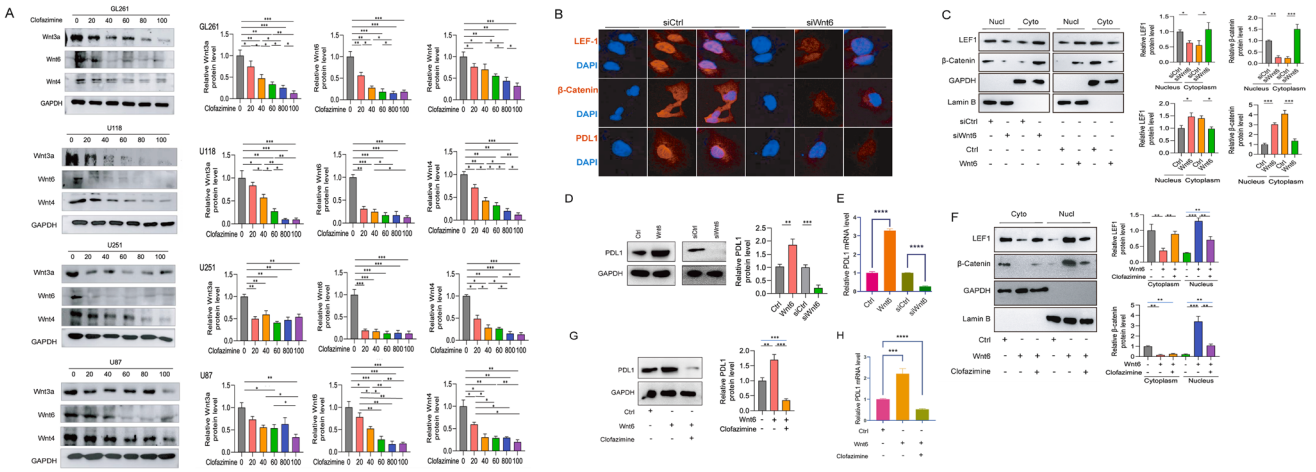

Fig. 3 Clofazimine inactivates the Wnt/β-catenin signaling by inhibiting Wnt6 expression in GBM cells. **A** Western blot analysis of Wnt6, Wnt3a, and Wnt4 expression in GBM cell lines treated with clofazimine. Wnt6 was the most sensitive to clofazimine treatment. **B**, **C** Western blot and immunofluorescence analysis of β-catenin and LEF-1 nuclear translocation in GBM cells with Wnt6 knockdown or overexpression. **D**, **E** Western blot and qRT-PCR analysis of PD-L1 expression in GBM cells with Wnt6 knockdown or overexpression. **F** Western blot analysis showing that Wnt6 overexpression rescued the clofazimine-mediated decrease in nuclear β-catenin and LEF-1. **G**, **H** Western blot and qRT-PCR analysis showing that Wnt6 overexpression rescued the clofazimine-mediated decrease in PD-L1 expression

and immunofluorescence analyses demonstrated that Wnt6 knockdown significantly inhibited the nuclear translocation of β-catenin and LEF-1, while Wnt6 overexpression resulted in increased nuclear translocation of these proteins (Fig. 3B and C). Additionally, Wnt6 modulation affected the protein and mRNA levels of PD-L1, with knockdown leading to decreased levels and overexpression resulting in increased levels (Fig. 3D and E).

Moreover, we observed that upregulation of Wnt6 significantly rescued the clofazimine-mediated decrease in the nuclear translocation of β-catenin and LEF-1 (Fig. 3F), as well as the protein and mRNA levels of PD-L1 (Fig. 3G and H). Collectively, these results suggest that clofazimine inhibits its PD-L1 expression by repressing Wnt6-induced activation of the Wnt/β-catenin signaling pathway.

Clofazimine inhibits human GBM cell proliferation and invasion by suppressing Wnt6-mediated activation of the Wnt/β-catenin pathway in vitro and in vivo

To further investigate the effects of clofazimine on human glioblastoma (GBM) cell proliferation and invasion, we focused on the regulatory mechanisms involving Wnt6. Our in vitro studies demonstrated that knockdown of Wnt6 significantly inhibited the proliferation of human GBM cells, as evidenced by reduced cell viability and increased apoptosis (Fig. 4A–F). Conversely, overexpression of Wnt6 led to enhanced cell proliferation and decreased apoptosis, highlighting the critical role of Wnt6 in GBM cell survival and growth.

Additionally, we assessed the impact of Wnt6 on GBM cell migration and invasion. Our results indicated that Wnt6 knockdown markedly suppressed these processes, while Wnt6 upregulation significantly enhanced cell migration and invasion capabilities (Fig. 4G–I). Notably, clofazimine treatment effectively inhibited the proliferation, migration, and invasion of GBM cells, and this effect was further potentiated by Wnt6 knockdown (Fig. 4J–N). Importantly, upregulation of Wnt6 was able to rescue the clofazimine-mediated inhibition of these cellular behaviors, suggesting that Wnt6 is a key mediator of clofazimine's effects.

To evaluate the in vivo effects of clofazimine on GBM progression, we established xenograft models using human GBM cells in nude mice. Tumor growth was monitored over time, and our findings revealed that Wnt6 upregulation significantly increased tumor volume compared to controls (Fig. 5A and B). In contrast, treatment with clofazimine effectively inhibited tumor growth, even in the presence of elevated Wnt6 levels, indicating that clofazimine can counteract the pro-tumorigenic effects of Wnt6 in vivo.

Furthermore, we noted that the combination of clofazimine with anti-PD-1 therapy resulted in enhanced therapeutic efficacy, as evidenced by a reduction in tumor volume, despite the observed upregulation of Wnt6 (Fig. 5D–G). Taken together, our findings demonstrate that clofazimine inhibits human GBM cell proliferation and invasion by suppressing Wnt6-mediated activation of the Wnt/β-catenin signaling pathway.

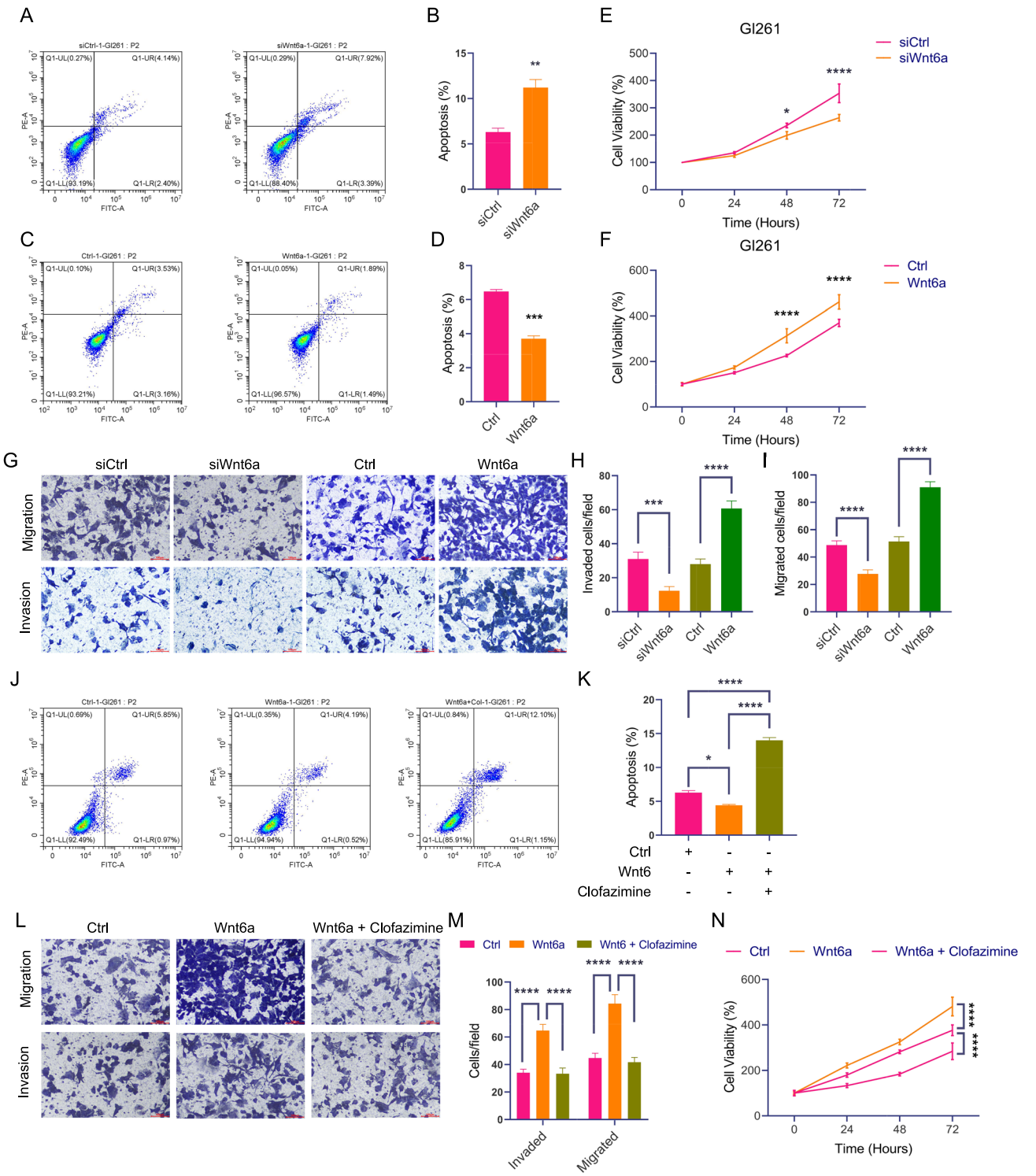

Fig. 4 Clofazimine inhibits human GBM cell proliferation and invasion in vitro. **A**–**F** Cell viability assays (**A**, **B**), Annexin V/PI staining (**C**, **D**), and representative flow cytometry plots (**E**, **F**) showing the effect of Wnt6 knockdown or overexpression on GBM cell proliferation and apoptosis. **G**–**I** Transwell migration (**G**) and invasion (**H**) assays and representative images (**I**) showing the effect of Wnt6 knockdown or overexpression on GBM cell migration and invasion. **J**–**N** Cell viability assays (**J**, **K**), Annexin V/PI staining (**L**, **M**), and representative flow cytometry plots (**N**) showing the combined effect of clofazimine and Wnt6 modulation on GBM cell proliferation and apoptosis

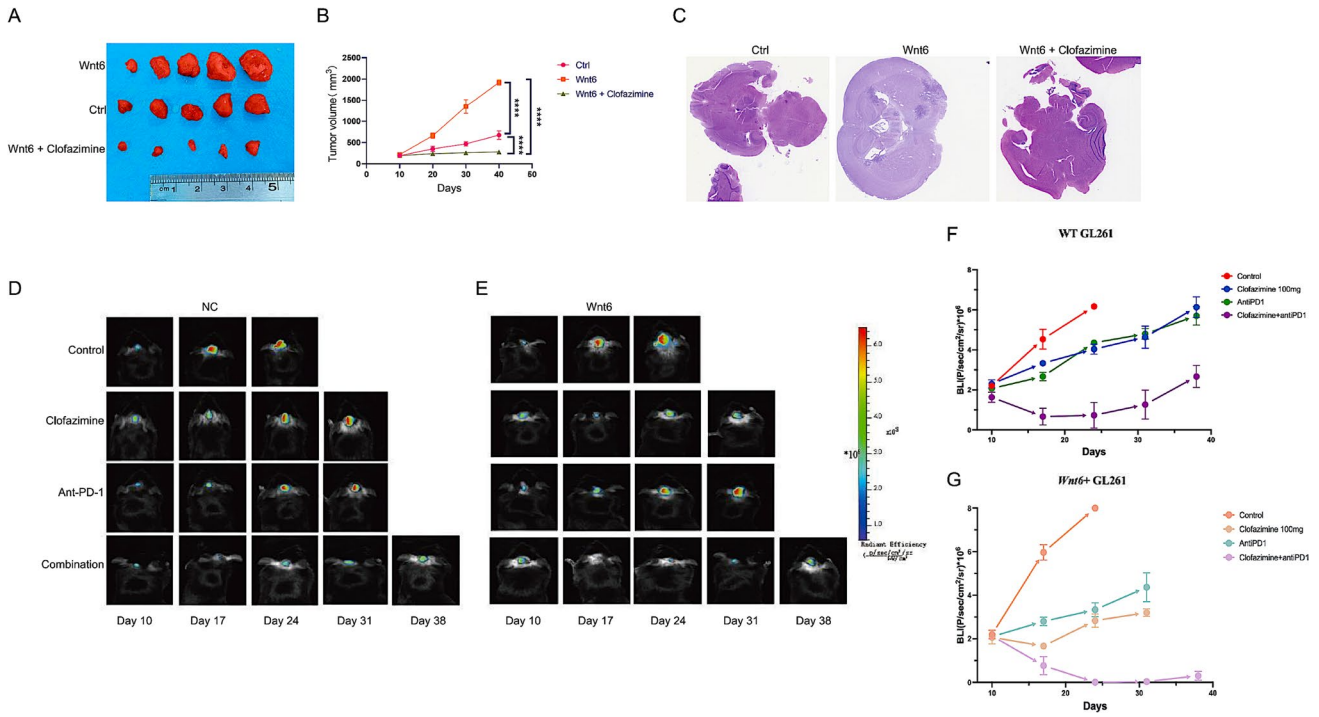

Fig. 5 Clofazimine inhibits human GBM cell proliferation and invasion in vivo. **A**, **B** Tumor growth curves in xenograft models using human GBM cells. Wnt6 upregulation increased tumor volume, while clofazimine treatment inhibited tumor growth. **C**–**G** Tumor volumes and representative images of tumors from mice treated with clofazimine, anti-PD-1, or the combination therapy. The combination therapy resulted in the smallest tumor volumes despite Wnt6 upregulation

Clofazimine enhances T cell activation and modulates the tumor immune microenvironment

To further elucidate the mechanisms underlying the enhanced antitumor efficacy of clofazimine in combination with anti-PD-1 therapy, we conducted an analysis of single-cell RNA sequencing data derived from the tumor microenvironment of treated mice. Our findings indicated that the combination therapy significantly increased the abundance of $CD8^+$ cytotoxic T cells and $CD4^+$ helper T cells compared to the control and monotherapy groups (Fig. 6A and B). Concurrently, we observed a marked reduction in the proportions of immunosuppressive Tregs and Th17 cells within the combination therapy cohort.

Moreover, we noted an upregulation in the expression of major histocompatibility MHC-II molecules on both tumor cells and antigen-presenting cells in mice undergoing combination therapy (Fig. 6C). This enhancement in MHC-II expression augments the antigen presentation capabilities, thereby facilitating more robust T-cell activation. Correspondingly, we evaluated the interactions of cytotoxic cytokine IFN—γ signaling pathway among cells in both combination group and anti-PD-1 group. As shown in the network diagram, B cells acted as key signaling hubs, interacting strongly with various cell types, and the interaction between T cells and macrophages was enhanced, which promoted T cell activity. This phenomenon was more significantly in the combination group, and other immune cells also participate more actively, which demonstrated that clofazimine combined with anti-PD-1 remarkably enhances the activation of the IFN-γ signaling pathway and promotes stronger interactions among immune cells, suggesting a more potent induction of tumor cell apoptosis (Fig. 6D). Immunofluorescence staining further corroborated these findings by highlighting increased infiltration of $CD3^+/CD8^+/PD\text{-}1^+$ T cells within the tumor stroma following the combined treatment (Fig. 6E–I). Additionally, flow cytometry analysis of peripheral blood samples revealed a similar trend, showing an increased proportion of circulating $CD3^+/CD8^+/PD\text{-}1^+$ T cells in mice treated with the combination therapy compared to both the control and monotherapy groups (Fig. 6J–M). Collectively, these results indicate that clofazimine effectively modulates the tumor immune microenvironment by promoting the infiltration and activation of cytotoxic T cells, while simultaneously facilitating antitumor macrophage polarization.

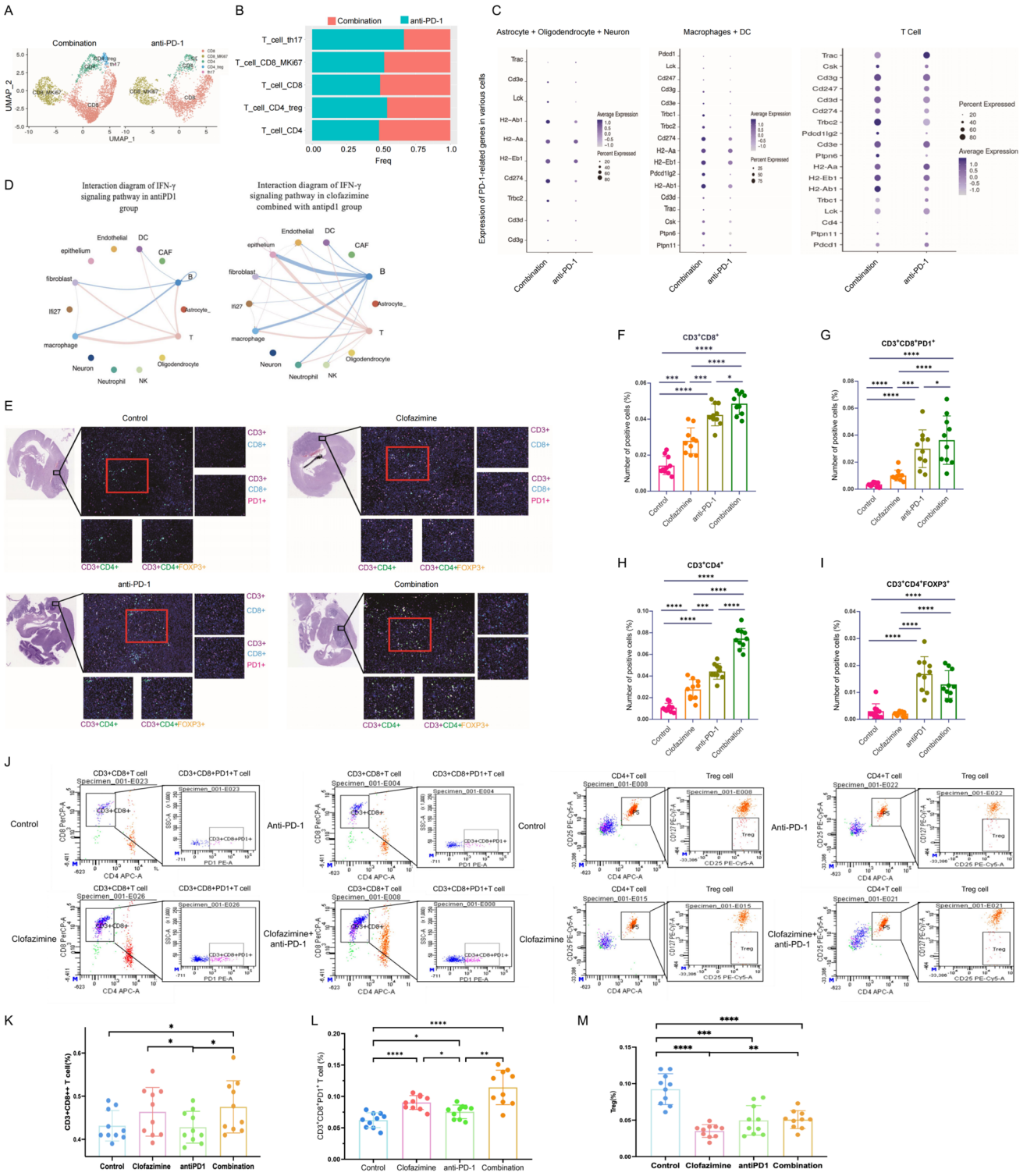

Fig. 6 Clofazimine enhances T cell activation and modulates the tumor immune microenvironment. **A**, **B** Single-cell RNA sequencing analysis showing the abundance of $CD8^+$ T cells (**A**) and $CD4^+$ T cells (**B**) in the tumor microenvironment of treated mice. **C** Heatmap showing differential expression of MHC-II molecules on tumor cells and antigen-presenting cells. D ELISA analysis of IFN-γ levels in tumor tissues. **E–I** Immunofluorescence staining for CD3, CD8, and PD-1 in tumor sections. The combination therapy increased the infiltration of $CD3^+/CD8^+/PD\text{-}1^+$ T cells. **J–M** Flow cytometry analysis of peripheral blood T cell subsets. The combination therapy increased the proportion of $CD3^+/CD8^+/PD\text{-}1^+$ T cells

Clofazimine enhances tumor-associated macrophage polarization and T cell receptor clonal diversity in the tumor microenvironment

In our subsequent investigations, we examined the impact of clofazimine on TAMs and the clonal diversity of TCRs within the tumor microenvironment. Analysis of single-cell RNA sequencing data revealed a significant increase in the proportion of pro-inflammatory M1 macrophages within the combination therapy group, known for their antitumorigenic properties, relative to the anti-PD-1 monotherapy group (Fig. 7A and B). Conversely, a marked reduction in the abundance of immunosuppressive M2 macrophages, which are typically associated with tumor progression and an immunosuppressive microenvironment, was observed in the same group (Fig. 7A–C). These findings strongly suggest that clofazimine effectively promotes macrophage polarization towards an antitumor phenotype, contributing to a more favorable immune landscape for combating tumor growth.

Additionally, the combination therapy resulted in notable enhancements in TCR clonal diversity among T cells. This improvement was evidenced by increased Shannon diversity and clonality indices in the peripheral blood of mice receiving clofazimine alongside anti-PD-1 therapy (Fig. 7D–F). The observed increase in TCR diversity implies a broader recognition of tumor-associated antigens, which is pivotal for mounting a robust and effective antitumor immune response. Furthermore, we identified a significantly higher proportion of shared TCR sequences in the combination therapy group (Fig. 7G–J), indicating a clonal expansion of T cells that specifically target tumor antigens. Collectively, these results underscore the role of clofazimine in enhancing both M1 macrophage polarization and TCR clonal diversity within the tumor microenvironment.

Discussion

The findings of our study provide compelling evidence that clofazimine, a Wnt/β-catenin signaling pathway inhibitor, significantly enhances the efficacy of anti-PD-1 immunotherapy in GBM (Fig. 8). In this study, the combination therapy with clofazimine and anti-PD-1 exerts anti-tumor effects through two mechanisms: 1) direct inhibition of tumor growth and invasion via Wnt6/β-catenin pathway suppression, leading to reduced tumor cell proliferation, increased apoptosis; and 2) reshaping the immune microenvironment, including enhanced CD8+ T cell infiltration, reduced Tregs,

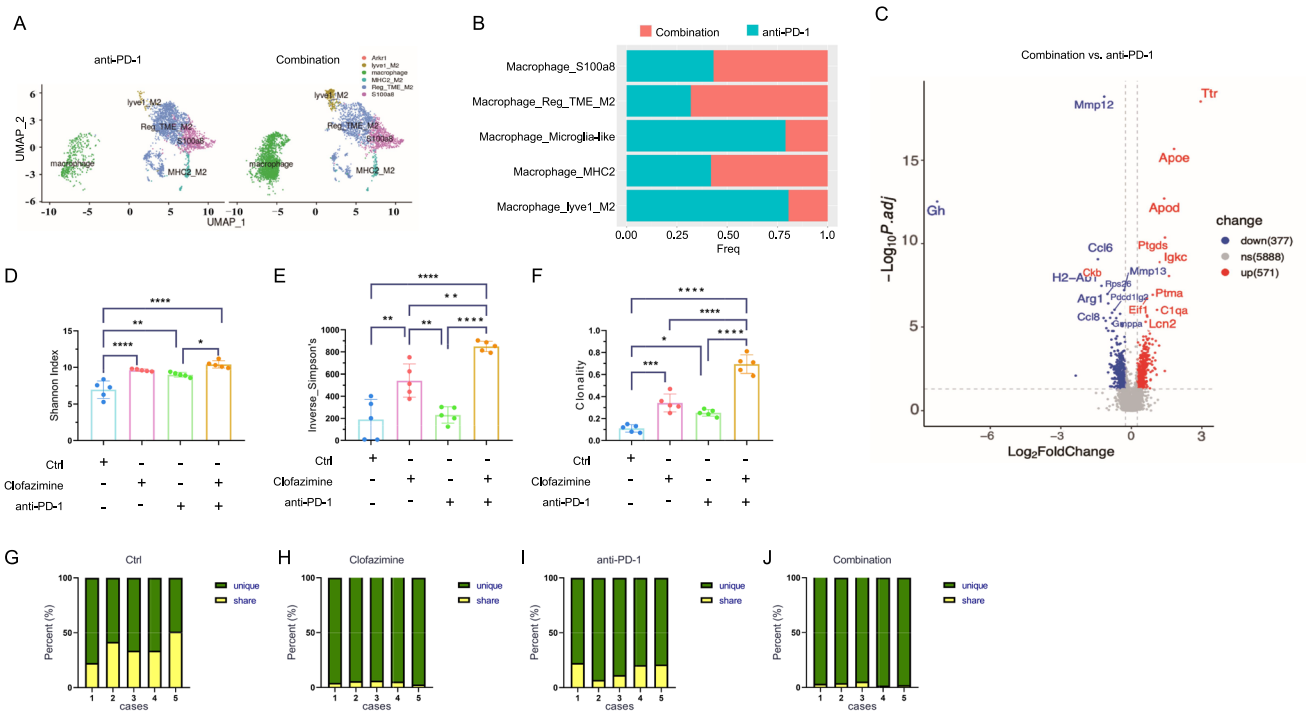

Fig. 7 Clofazimine enhances tumor-associated macrophage polarization and T cell receptor clonal diversity. **A**, **B** Single-cell RNA sequencing analysis showing the proportion of M1 (**A**) and M2 (**B**) macrophages in the tumor microenvironment. **C** Heatmap showing differential expression of M1 and M2 macrophage markers. **D–F** TCR diversity indices (Shannon entropy and Simpson's diversity index) in peripheral blood of treated mice. The combination therapy increased TCR clonal diversity. **G–J** Venn diagrams showing shared TCR sequences between treatment groups. The combination therapy had a higher proportion of shared TCR sequences, indicating clonal expansion of tumor-specific T cells

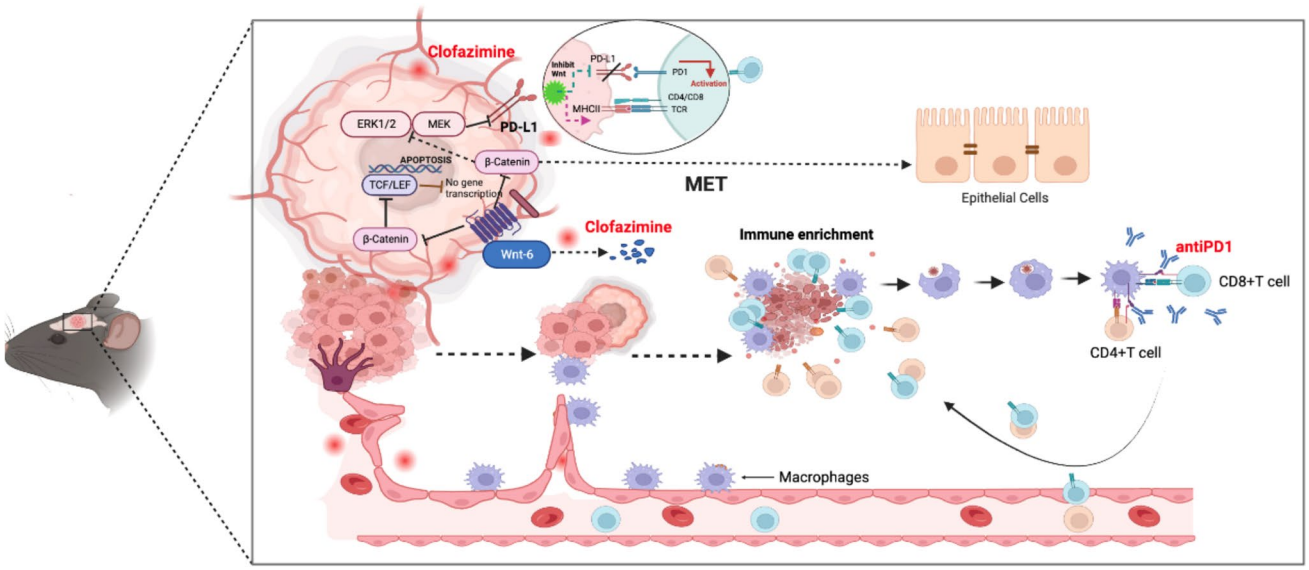

Fig. 8 Clofazimine enhances the therapeutic effect of anti-PD1 by inhibiting the Wnt pathway, reducing the expression of PDL1, and improving the tumor immune microenvironment

promoted M1 macrophage polarization, and improved TCR clonal diversity. The downregulation of PD-L1 further alleviates T cell suppression, while anti-PD-1 enhances the immune activation effect, leading to synergistic anti-tumor activity. This dual mechanism results in significant tumor growth inhibition and prolonged survival in pre-clinical models. This is particularly relevant given the current challenges in treating GBM, where conventional therapies often fail due to the tumor's aggressive nature and its immunosuppressive microenvironment. Our results align with recent literature that emphasizes the need for innovative strategies to overcome the limitations of immunotherapy in GBM.

Previous studies have highlighted the immunosuppressive characteristics of the GBM microenvironment, which is enriched with Tregs [26], MDSCs [27], and M2-polarized TAMs [28]. These factors contribute to the poor response to ICIs such as anti-PD-1. Our findings that clofazimine treatment resulted in a significant increase in cytotoxic $CD8^+$ T cell infiltration and a reduction in Tregs corroborate the observations made by other researchers who have noted similar shifts in immune cell populations following the modulation of the TME [29]. The ability of clofazimine to reshape the immune landscape of GBM tumors is a critical advancement, as it suggests a potential pathway to convert 'cold' tumors into 'hot' tumors, which are more responsive to immunotherapy.

In GBM, PD-L1 expression may indicate immune evasion rather than immune activation. While PD-L1 upregulation in "hot tumors," such as lung cancer, typically reflects active immune responses and is a predictive marker for anti-PD-1 therapy, the immune microenvironment in GBM is highly immunosuppressive. Factors such as the accumulation of immune-suppressive cells, low tumor mutation burden, and the blood–brain barrier limit the effectiveness of T cell responses and immune therapy. Furthermore, activation of the Wnt/β-catenin pathway in GBM may impair antigen presentation, further contributing to immune evasion. Therefore, PD-L1 upregulation in GBM is more likely a marker of immune resistance, explaining the limited efficacy of anti-PD-1 monotherapy in this context. Moreover, our study demonstrates that clofazimine not only reduces PD-L1 expression through the downregulation of Wnt6-mediated activation of the Wnt/β-catenin pathway but also inhibits EMT, a process known to contribute to immune evasion [30, 31]. This finding is particularly significant in light of recent research that has identified EMT as a mechanism by which tumors escape immune surveillance [32]. By targeting both the Wnt pathway and EMT, clofazimine has the potential to enhance the anti-tumor immune response in GBM, providing a promising therapeutic strategy that may overcome immune resistance and improve the efficacy of anti-PD-1 therapy.

In contrast to the limited success of anti-PD-1 monotherapy in GBM, our combination therapy with clofazimine resulted in a marked reduction in tumor growth and improved survival in orthotopic GBM mouse models. This is consistent with findings from studies that have explored combination therapies in other malignancies, suggesting that the synergistic effects of combining ICIs with agents targeting tumor-intrinsic pathways can lead to improved therapeutic outcomes [33]. The enhanced survival observed in our study, particularly in Wnt6-transfected models, further

supports the notion that targeting specific signaling pathways can potentiate the effects of immunotherapy.

Interestingly, while our results indicate a significant increase in M1 macrophage populations following clofazimine treatment, we also observed a complex interplay with M2 macrophages. The reduction in M2 macrophages, particularly the regulatory subtype, aligns with literature suggesting that M2 macrophages contribute to tumor progression and immune suppression [34–36] However, the increase in certain M2 subsets raises questions about the dual roles of macrophages in the TME and their potential involvement in tissue repair and immune regulation [37]. This complexity underscores the need for further investigation into the functional roles of macrophage subtypes in the context of GBM therapy.

In summary, our study highlights the potential of clofazimine as a novel therapeutic agent that can enhance the efficacy of anti-PD-1 immunotherapy in GBM by modulating the Wnt/β-catenin/PD-L1 axis and reshaping the immunosuppressive microenvironment. As we continue to unravel the intricate dynamics of the TME and its impact on immunotherapy, our results suggest that targeting specific signaling pathways may be a promising strategy to improve patient outcomes in this challenging malignancy. Although our study demonstrates promising results in pre-clinical mouse models, the therapeutic effects of clofazimine combined with anti-PD-1 therapy need to be validated in clinical trials to determine their applicability in human patients. The dosage of clofazimine used in mice may not directly translate to humans, and further studies are needed to determine the optimal treatment regimen. Moreover, the safety and potential toxicity of combining clofazimine with anti-PD-1 therapy require thorough investigation in clinical settings. Finally, while our study focused on immune cell infiltration and macrophage polarization, a more comprehensive understanding of the tumor microenvironment's complexity and the roles of other immune and stromal cells is needed for a complete assessment of the treatment's impact.

Methods and materials

Cell culture and treatments

Glioblastoma multiforme (GBM) cell lines GL261, U87, U118, and U251 were obtained from the American Type Culture Collection (ATCC, USA). GL261 cells were cultured in Dulbecco's Modified Eagle Medium (DMEM; Thermo Fisher Scientific, USA) supplemented with 10% fetal bovine serum (FBS; Gibco, USA) and 1% penicillin–streptomycin (Thermo Fisher Scientific, USA). U87, U118, and U251 cells were maintained under similar conditions. All cells were incubated at 37 °C in a humidified atmosphere containing 5% CO_2.

For treatment experiments, cells were seeded in appropriate culture plates and allowed to adhere overnight. Clofazimine (Sigma-Aldrich, USA) was dissolved in dimethyl sulfoxide (DMSO; Sigma-Aldrich, USA) to create a stock solution. Working concentrations of clofazimine were prepared by diluting the stock solution in culture medium to final concentrations of 0, 20, 40, 60, 80, or 100 μM. Control groups received an equivalent volume of DMSO. Cells were treated for specified durations depending on the subsequent assays.

Quantitative real-time PCR (qRT-PCR)

Total RNA was extracted from cells using TRIzol™ Reagent (Invitrogen, USA) according to the manufacturer's instructions. The concentration and purity of RNA were measured using a NanoDrop™ spectrophotometer (Thermo Fisher Scientific, USA). Complementary DNA (cDNA) was synthesized from 2 μg of total RNA using the Maxima H Minus cDNA Synthesis Master Mix (Thermo Fisher Scientific, USA).

Quantitative PCR was performed using the Power SYBR™ Green RNA-to-CT™ 1-Step Kit (Applied Biosystems, USA) on an Applied Biosystems QuantStudio™ real-time PCR system. The specific primers for Wnt3a, Wnt6, β-catenin, c-Myc, E-cadherin, Vimentin, and β-actin (internal control) are listed in Supplementary Table 1. The thermal cycling conditions were set as per the kit's protocol. The relative gene expression levels were calculated using the $2^{-\Delta\Delta CT}$ method.

Immunocytochemistry and immunofluorescence (ICC/IF) assays

GL261 cells were seeded onto sterile glass coverslips placed in 24-well plates and cultured overnight. Cells were then treated with clofazimine at concentrations of 0, 20, 40, 60, 80, or 100 μM for 48 h. After treatment, cells were fixed with 4% paraformaldehyde (Sigma-Aldrich, USA) for 15 min at room temperature and permeabilized with 0.5% Triton™ X-100 (Sigma-Aldrich, USA) for 10 min. Following three washes with phosphate-buffered saline (PBS; Thermo Fisher Scientific, USA), cells were blocked with 5% bovine serum albumin (BSA; Sigma-Aldrich, USA) for 1 h at room temperature.

Primary antibodies (Supplementary Table 2) were diluted in blocking solution and applied to the cells overnight at 4 °C. After washing with PBS, cells were incubated with appropriate fluorescently labeled secondary antibodies (Abcam, USA) for 1 h at room temperature in the dark. Nuclei were counterstained with DAPI

(Sigma-Aldrich, Italy). Images were captured using an Olympus fluorescence microscope (Olympus Corporation, Japan) equipped with appropriate filters.

Cell transfection and lentiviral infection

Lentiviral plasmids for Wnt6 overexpression and control vectors were obtained from Hanbio Biotechnology Co., Ltd. (Shanghai, China). GL261, U87, U118, and U251 cells were transfected using Lipofectamine™ 3000 Transfection Reagent (Invitrogen, USA) following the manufacturer's protocol. Briefly, cells were seeded to reach 70–80% confluency at the time of transfection. Plasmid DNA and Lipofectamine 3000 reagent were mixed in Opti-MEM™ Reduced Serum Medium (Thermo Fisher Scientific, USA) to form transfection complexes, which were then added to the cells. After 6 h, the medium was replaced with fresh complete medium.

For lentiviral infection, cells were transduced with lentiviral particles in the presence of polybrene (8 μg/mL; Sigma-Aldrich, USA) to enhance transduction efficiency. Cells were selected with puromycin (2 μg/mL; Sigma-Aldrich, USA) for 7 days to establish stable cell lines. Transfection and infection efficiencies were confirmed by qRT-PCR and Western blot analysis.

Western blot analysis

Cells were lysed using RIPA buffer (Sigma-Aldrich, USA) supplemented with protease inhibitors (Complete™ Mini EDTA-free Protease Inhibitor Cocktail Tablets; Roche, Germany). Protein concentrations were determined using the Pierce™ BCA Protein Assay Kit (Thermo Fisher Scientific, USA). Equal amounts of protein (30 μg per sample) were separated by SDS-PAGE using 10% polyacrylamide gels and then transferred onto PVDF membranes (Immobilon®-P; Millipore, USA).

Membranes were blocked with 5% BSA in Tris-buffered saline containing 0.1% Tween® 20 (TBST; Sigma-Aldrich, USA) for 1 h at room temperature and incubated overnight at 4 °C with primary antibodies (listed in Supplementary Table 1). After washing with TBST, membranes were incubated with horseradish peroxidase (HRP)-conjugated secondary antibodies (Jackson ImmunoResearch Laboratories, USA) for 1 h at room temperature. Protein bands were detected using the ECL™ Western Blotting Detection Reagent (GE Healthcare, USA) and visualized with the ChemiDoc™ XRS + System (Bio-Rad Laboratories, USA). Densitometric analysis was performed using Image Lab™ Software (Bio-Rad Laboratories, USA), with GAPDH serving as the loading control.

Flow cytometry

Apoptosis analysis

Wild-type GL261 cells were treated with various concentrations of clofazimine or DMSO for 24 h. Cells were harvested, washed twice with cold PBS, and resuspended in Annexin V binding buffer (Invitrogen, USA). Annexin V-PE and propidium iodide (PI) staining was performed using the Annexin V Apoptosis Detection Kit (Invitrogen, USA) according to the manufacturer's instructions. Samples were analyzed on a Beckman Coulter FC500 flow cytometer (Beckman Coulter, USA), and data were processed using CytExpert™ Software (Beckman Coulter, USA).

T cell phenotyping

Peripheral blood was collected from treated mice via submandibular bleeding. Red blood cells were lysed using RBC Lysis Buffer (eBioscience™, USA). Remaining cells were washed and incubated with fluorochrome-conjugated antibodies specific for CD3 (FITC-labeled, clone 17A2), CD4 (PerCP-Cy5.5-labeled, clone RM4-5), CD8 (APC-labeled, clone 53–6.7), PD-1 (PE-labeled, clone J43), and intracellular Foxp3 (PE-Cy7-labeled, clone FJK-16 s) (all antibodies from BD Biosciences, USA or eBioscience™, USA). Intracellular staining for Foxp3 was performed using the Foxp3/Transcription Factor Staining Buffer Set (eBioscience™, USA). Samples were analyzed on the FC500 flow cytometer, and data were analyzed with FlowJo™ Software (BD Biosciences, USA).

Transwell migration and invasion assays

Cell migration and invasion were assessed using Transwell® chambers with 8 μm pore polycarbonate membranes (Corning Costar, USA). For migration assays, GL261 cells (5×10^4 cells per well) treated with clofazimine were resuspended in serum-free DMEM and added to the upper chamber. For invasion assays, the upper chambers were pre-coated with Matrigel® Basement Membrane Matrix (BD Biosciences, USA) diluted 1:8 in serum-free DMEM, and 1×10^5 cells were seeded.

The lower chambers were filled with DMEM containing 10% FBS as a chemoattractant. After 24 h of incubation at 37 °C in 5% CO_2, non-migrated/non-invaded cells on the upper surface of the membranes were gently removed with cotton swabs. Cells that had migrated or invaded to the lower surface were fixed with methanol (Sigma-Aldrich, USA) for 15 min, stained with 0.1% crystal violet (Sigma-Aldrich, USA) for 20 min, and rinsed with distilled water. Cells were counted in five randomly selected fields per membrane under an inverted microscope (Olympus Corporation, Japan).

Mouse orthotopic GBM models and treatments

All animal experiments were approved by the Experimental Animal Welfare Ethics Committee of Beijing Yongxin Kangtai Technology Development Co., Ltd. (approval number YXKT2023L022) and conducted in accordance with institutional guidelines. This study was conducted in full compliance with the ARRIVE guidelines to ensure the transparency, reproducibility, and ethical integrity of our research. Female C57BL/6 mice (5 weeks old) were purchased from the Beijing Vital River Laboratory Animal Technology Co., Ltd. (Beijing, China) and housed under specific pathogen-free (SPF) conditions with a 12-h light/dark cycle and free access to food and water.

For the establishment of orthotopic GBM models, mice were anesthetized with isoflurane (RWD Life Science Co., Ltd., China) and positioned in a stereotactic frame (RWD Life Science Co., Ltd., China). GL261-LUC cells (5×10^5 cells in 2 µL PBS) were slowly injected over 5 min into the right striatum at the following coordinates: 2 mm lateral to the bregma, 1 mm anterior, 3 mm depth from the skull surface.

Mice were randomly assigned to four groups (n = 20 per group): 1) Control Group: Received vehicle (0.5% DMSO in PBS) orally and intraperitoneal injections of isotype control antibody (IgG). 2) Clofazimine Monotherapy Group: Treated with clofazimine (100 mg/kg/day, orally via gavage; Sigma-Aldrich, USA) and intraperitoneal injections of isotype control antibody. 3) Anti-PD-1 Monotherapy Group: Received vehicle orally and anti-PD-1 antibody (12.5 mg/kg, intraperitoneal injection every three days; clone RMP1-14, Bio X Cell, USA). 4) Combination Therapy Group: Treated with clofazimine (as above) and anti-PD-1 antibody (as above).

Treatments commenced on day 11 post-tumor implantation and continued for 14 days. Tumor growth was monitored by bioluminescence imaging using the IVIS Spectrum System (PerkinElmer, USA). Mice were anesthetized with isoflurane and injected intraperitoneally with D-luciferin potassium salt (150 mg/kg; PerkinElmer, USA) 10 min prior to imaging. Bioluminescence signals were quantified using Living Image® Software (PerkinElmer, USA).

Xenograft models and treatment protocols

Xenograft models were established using U87 glioma cells, which were transfected with Wnt6 or left wild-type (WT). Briefly, U87 cells ($5 \times 10^{\wedge 5}$) in 100 µL of PBS were subcutaneously injected into the flanks of immunocompromised mice per group (n = 8). The groups included: (1) Wnt6-transfected group, (2) wild-type (WT) group, and (3) Wnt6-transfected + clofazimine-treated group. For the Wnt6-transfected + clofazimine-treated group, mice were administered clofazimine (100 mg/kg/day) orally, starting from day 10 post-injection. The treatment regimen was continued every day for a total of 40 days. Tumor growth was monitored by measuring tumor size every 5 days using calipers, and tumor volume was calculated according to the formula: Volume = (Length × Width^2) / 2. Mice were sacrificed at 10, 20, 30, and 40 days post-injection, and tumor tissues were excised for histological analysis and further measurements. Tumor sizes were plotted for each time point (10, 20, 30, and 40 days) to assess the therapeutic effects of the treatments. Tumor volume data were statistically analyzed to compare differences between groups.

Immunohistochemistry and immunofluorescence staining of mouse brain tissue

Mice were euthanized at designated time points post-treatment. Whole brains were harvested and fixed in 4% paraformaldehyde (Sigma-Aldrich, USA) at 4 °C overnight. Tissues were dehydrated, embedded in paraffin, and sectioned into 5 µm coronal slices using a microtome (Leica Microsystems, Germany).

Hematoxylin and Eosin (H&E) staining

Sections were deparaffinized in xylene and rehydrated through a graded ethanol series to distilled water. H&E staining was performed using standard protocols to evaluate histopathological changes.

Immunohistochemistry (IHC)

Tissue sections underwent antigen retrieval by heating in citrate buffer (10 mM sodium citrate, pH 6.0) using a microwave oven for 15 min. Endogenous peroxidase activity was blocked by incubating sections in 3% hydrogen peroxide (Sigma-Aldrich, USA) for 10 min. After blocking with 10% normal goat serum (Vector Laboratories, USA) for 1 h at room temperature, sections were incubated overnight at 4 °C with primary antibodies (see Supplementary Table 2).

The following day, sections were washed and incubated with biotin-conjugated secondary antibodies (Vector Laboratories, USA) for 1 h at room temperature. Visualization was achieved using the VECTASTAIN® ABC Kit and DAB Peroxidase Substrate Kit (Vector Laboratories, USA). Sections were counterstained with hematoxylin, dehydrated, cleared, and mounted with Permount™ Mounting Medium (Thermo Fisher Scientific, USA).

Immunofluorescence (IF) staining

For IF staining, after antigen retrieval and blocking as described above, sections were incubated with primary

antibodies overnight at 4 °C. After washing, sections were incubated with fluorophore-conjugated secondary antibodies (Invitrogen, USA) for 1 h at room temperature in the dark. Nuclei were counterstained with DAPI. Slides were mounted using ProLong™ Gold Antifade Reagent (Thermo Fisher Scientific, USA). Imaging was performed using a fluorescence microscope (Olympus Corporation, Japan). Negative controls without primary antibodies were included to assess nonspecific staining.

Single-cell RNA sequencing and data analysis

Single-cell suspensions were prepared from freshly harvested tumor tissues using the Tumor Dissociation Kit (Miltenyi Biotec, Germany) and gentleMACS™ Dissociator (Miltenyi Biotec, Germany) following the manufacturer's instructions. Cell suspensions were filtered through a 70 µm cell strainer (Falcon, Corning, USA) and centrifuged at 300× g for 10 min at 4 °C. Dead cells were removed using the Dead Cell Removal Kit (Miltenyi Biotec, Germany). Cell viability (> 90%) was confirmed using the Trypan Blue Stain (Thermo Fisher Scientific, USA) and Countess™ II Automated Cell Counter (Thermo Fisher Scientific, USA).

Single-cell RNA sequencing libraries were generated using the Chromium™ Single Cell 3′ Reagent Kit v3 (10× Genomics, USA) according to the manufacturer's protocol. Libraries were sequenced on the Illumina NovaSeq 6000 platform (Illumina, USA) to obtain high-depth sequencing data.

Data processing was performed using Cell Ranger software (v3.1, 10× Genomics, USA) for demultiplexing, read alignment to the mouse reference genome (mm10), and gene counting. Further analyses were conducted in R using the Seurat package (v3.1). Quality control excluded cells with fewer than 200 genes, more than 5,000 genes, or mitochondrial gene content exceeding 10%. Normalization, scaling, and principal component analysis (PCA) were conducted. Cell clustering was performed using the shared nearest neighbor (SNN) method, and clusters were visualized using Uniform Manifold Approximation and Projection (UMAP). Cell types were annotated based on canonical marker genes. Differential gene expression analyses utilized the Wilcoxon rank-sum test, and functional enrichment analyses employed the clusterProfiler R package.

T cell receptor (TCR) sequencing

Peripheral blood mononuclear cells (PBMCs) were isolated from mouse blood samples using Ficoll-Paque™ Plus (GE Healthcare, USA) density gradient centrifugation. Genomic DNA was extracted using the DNeasy® Blood & Tissue Kit (Qiagen, Germany) per the manufacturer's protocol.

The complementarity-determining region 3 (CDR3) of TCR β-chain was amplified using the Mouse TCRβ Profiling Kit (iRepertoire®, USA), which employs a multiplex PCR strategy covering all Vβ and Jβ segments. Amplified products were purified using AMPure XP beads (Beckman Coulter, USA) and quantified using Qubit™ dsDNA HS Assay Kit (Thermo Fisher Scientific, USA). Libraries were sequenced on an Illumina MiSeq™ platform (Illumina, USA) with 300 bp paired-end reads.

Raw sequencing data were processed using the iRweb software (iRepertoire®, USA) to assemble TCR sequences and quantify clonotypes. Clonality and diversity indices, such as Shannon entropy and Simpson's diversity index, were calculated using VDJtools software. Comparative analyses of TCR repertoires between groups were performed to assess clonal expansion and diversity changes resulting from treatments.

Statistical analysis

Experimental data are presented as mean ± standard deviation (SD) from at least three independent experiments. Statistical analyses were performed using GraphPad Prism 8.0 software (GraphPad Software, USA). Differences between two groups were evaluated using unpaired two-tailed Student's t-tests. Multiple group comparisons were conducted using one-way analysis of variance (ANOVA) followed by Tukey's post hoc test. Survival curves were generated using the Kaplan–Meier method and compared using the log-rank (Mantel-Cox) test. A p-value of less than 0.05 was considered statistically significant.

Supplementary Information The online version contains supplementary material available at https://doi.org/10.1007/s00262-025-03994-5.

Author contributions Yuze Zhao: data curation—managed the acquisition and validation of datasets; investigation—conducted primary experimental work; methodology—developed analytical methods and experimental designs; writing—original draft—drafted the initial manuscript. Yuguang Song: data curation—assisted in the management of data; resources—provided essential materials and tools for the research. Weiping Li: data curation—supported data collection and management; methodology—contributed to the development of new methods. Jiangping Wu: methodology—co-developed the research methodology; software—created and maintained software tools necessary for the analysis. Zhengbao Zhao: investigation—played a pivotal role in experimental research; supervision—oversaw the research project and provided guidance. Tingli Qu: methodology—participated in the development of methods; project administration—managed project operations and logistics. Hong Xiao: software—developed software solutions for data analysis; methodology—collaborated on methodological enhancements. Manyuan Wang: methodology—contributed to method development; formal analysis—conducted complex statistical analysis. Min Zhu: formal analysis—performed statistical analysis and data interpretation; methodology—Assisted in refining analytical methods. Peiming Zheng: methodology—involved in the development and execution of methodologies. Huili Wan: methodology—engaged in methodological improvements and implementations. Qingkun

Song: methodology—assisted in methodological development and refinement; resources—supplied critical resources and infrastructure. Funding acquisition—acquisition of the financial support for the project leading to this publication. Huixia Zheng: conceptualization—led the conceptualization of the research theme; data curation—managed comprehensive datasets; methodology—devised and refined research methodologies; supervision—provided strategic leadership and oversight. Shuo Wang: conceptualization—co-led the design and framework of the study; data curation—assisted in data management and verification; formal analysis—conducted key statistical and analytical reviews; validation—verified the accuracy and replicability of results; writing—review and editing—critically reviewed and edited the manuscript for intellectual content.

Funding This work was supported by the Beijing research center for respiratory infectious diseases project (BJRID2024-001) and Beijing Shijitan Hospital Youth Found (2023-q08). The funder of this research is Song Qingkun, who is one of our co-corresponding authors. This research project mainly centers around the study of respiratory infectious diseases. In particular, we are exploring the potential of Clofazimine, a drug conventionally used for treating tuberculosis, for its therapeutic effects in tumors. Mr. Song Qingkun provided the funding to support this innovative research. Although the funding source may not seem to directly match the authors' institutions, it is due to the nature of this exploratory research project that aims to bridge the gap between different medical fields and uncover new therapeutic applications.

Data availability The data generated and analyzed during the current study are available from the corresponding authors upon reasonable request. The raw data, including but not limited to in vitro and in vivo experimental results, single-cell RNA sequencing data, flow cytometry analysis, and immunohistochemistry images, have been meticulously documented and archived for future reference. Due to privacy concerns and ethical restrictions related to patient data and animal studies, certain raw data may not be publicly available. However, we are committed to sharing processed data, statistical analyses, and detailed methodologies to facilitate reproducibility and further research in the field. Interested researchers are invited to contact the corresponding authors.

Declarations

Conflict of interest The authors declare no competing interests.

Ethical approval In our study, the animal experiments were conducted in a collaborating company instead of our hospital. This was because our hospital's animal facility was under renovation at that time. The collaborating company is specialized in animal experiments and holds the necessary qualifications. It is also registered as a collaborating institution with our hospital. The animal ethics application was submitted and approved through the proper channels within this company, ensuring that all procedures adhered to ethical guidelines and regulations.

References

1. Wu W et al (2021) Glioblastoma multiforme (GBM): an overview of current therapies and mechanisms of resistance. Pharmacol Res. 171:105780. https://doi.org/10.1016/j.phrs.2021.105780
2. Czarnywojtek A et al (2023) Glioblastoma multiforme: the latest diagnostics and treatment techniques. Pharmacology 108:423–431. https://doi.org/10.1159/000531319
3. Grochans S et al (2022) Epidemiology of glioblastoma multiforme-literature review. Cancers (Basel). https://doi.org/10.3390/cancers14102412
4. Bikfalvi A et al (2023) Challenges in glioblastoma research: focus on the tumor microenvironment. Trends Cancer 9:9–27. https://doi.org/10.1016/j.trecan.2022.09.005
5. Yasinjan F et al (2023) Immunotherapy: a promising approach for glioma treatment. Front Immunol. 14:1255611. https://doi.org/10.3389/fimmu.2023.1255611
6. Reck M, Remon J, Hellmann MD (2022) First-line immunotherapy for non-small-cell lung cancer. J Clin Oncol. 40:586–597. https://doi.org/10.1200/JCO.21.01497
7. Marei HE, Hasan A, Pozzoli G, Cenciarelli C (2023) Cancer immunotherapy with immune checkpoint inhibitors (ICIs): potential, mechanisms of resistance, and strategies for reinvigorating T cell responsiveness when resistance is acquired. Cancer Cell Int. 23:64. https://doi.org/10.1186/s12935-023-02902-0
8. Reardon DA et al (2020) Effect of nivolumab vs bevacizumab in patients with recurrent glioblastoma: the CheckMate 143 phase 3 randomized clinical trial. JAMA Oncol. 6:1003–1010. https://doi.org/10.1001/jamaoncol.2020.1024
9. Omuro A et al (2023) Radiotherapy combined with nivolumab or temozolomide for newly diagnosed glioblastoma with unmethylated MGMT promoter: An international randomized phase III trial. Neuro Oncol. 25:123–134. https://doi.org/10.1093/neuonc/noac099
10. Lin H et al (2024) Understanding the immunosuppressive microenvironment of glioma: mechanistic insights and clinical perspectives. J Hematol Oncol. 17:31. https://doi.org/10.1186/s13045-024-01544-7
11. Vafaei S et al (2022) Combination therapy with immune checkpoint inhibitors (ICIs); a new frontier. Cancer Cell Int. 22:2. https://doi.org/10.1186/s12935-021-02407-8
12. Lee Y, Lee JK, Ahn SH, Lee J, Nam DH (2016) WNT signaling in glioblastoma and therapeutic opportunities. Lab Invest. 96:137–150. https://doi.org/10.1038/labinvest.2015.140
13. Barzegar Behrooz A et al (2022) Wnt and PI3K/Akt/mTOR survival pathways as therapeutic targets in glioblastoma. Int J Mol Sci. https://doi.org/10.3390/ijms23031353
14. Lim SH et al (2024) PLD1 is a key player in cancer stemness and chemoresistance: therapeutic targeting of cross-talk between the PI3K/Akt and Wnt/beta-catenin pathways. Exp Mol Med. 56:1479–1487. https://doi.org/10.1038/s12276-024-01260-9
15. Hasan S, Mahmud Z, Hossain M, Islam S (2024) Harnessing the role of aberrant cell signaling pathways in glioblastoma multiforme: a prospect towards the targeted therapy. Mol Biol Rep. 51:1069. https://doi.org/10.1007/s11033-024-09996-3
16. Zhou Y et al (2022) Wnt signaling pathway in cancer immunotherapy. Cancer Lett. 525:84–96. https://doi.org/10.1016/j.canlet.2021.10.034
17. Xu J, Koval A, Katanaev VL (2020) Beyond TNBC: repositioning of clofazimine against a broad range of Wnt-dependent cancers.

Front Oncol. 10:602817. https://doi.org/10.3389/fonc.2020.602817
18. Goncalves CS et al (2020) A novel molecular link between HOXA9 and WNT6 in glioblastoma identifies a subgroup of patients with particular poor prognosis. Mol Oncol. 14:1224–1241. https://doi.org/10.1002/1878-0261.12633
19. Zheng H et al (2010) PLAGL2 regulates Wnt signaling to impede differentiation in neural stem cells and gliomas. Cancer Cell 17:497–509. https://doi.org/10.1016/j.ccr.2010.03.020
20. Desterke C et al (2025) Single-cell RNA sequencing reveals LEF1-driven Wnt pathway activation as a shared oncogenic program in hepatoblastoma and medulloblastoma. Curr Oncol. https://doi.org/10.3390/curroncol32010035
21. Cruciat CM (2014) Casein kinase 1 and Wnt/beta-catenin signaling. Curr Opin Cell Biol. 31:46–55. https://doi.org/10.1016/j.ceb.2014.08.003
22. Hiremath M et al (2012) Parathyroid hormone-related protein activates Wnt signaling to specify the embryonic mammary mesenchyme. Development 139:4239–4249. https://doi.org/10.1242/dev.080671
23. Bell I et al (2024) Nkd1 functions downstream of Axin2 to attenuate Wnt signaling. Mol Biol Cell. 35:ar93. https://doi.org/10.1091/mbc.E24-02-0059-T
24. Shi Y et al (2022) Interaction between BEND5 and RBPJ suppresses breast cancer growth and metastasis via inhibiting Notch signaling. Int J Biol Sci. 18:4233–4244. https://doi.org/10.7150/ijbs.70866
25. Zhang S, Wang Y, Dai SD, Wang EH (2011) Down-regulation of NKD1 increases the invasive potential of non-small-cell lung cancer and correlates with a poor prognosis. BMC Cancer 11:186. https://doi.org/10.1186/1471-2407-11-186
26. Amoozgar Z et al (2021) Targeting Treg cells with GITR activation alleviates resistance to immunotherapy in murine glioblastomas. Nat Commun. 12:2582. https://doi.org/10.1038/s41467-021-22885-8
27. Zannikou M et al (2023) IL15 modification enables CAR T cells to act as a dual targeting agent against tumor cells and myeloid-derived suppressor cells in GBM. J Immunother Cancer. https://doi.org/10.1136/jitc-2022-006239
28. Khan F et al (2023) Macrophages and microglia in glioblastoma: heterogeneity, plasticity, and therapy. J Clin Invest. https://doi.org/10.1172/JCI163446
29. Xue G et al (2024) Clinical drug screening reveals clofazimine potentiates the efficacy while reducing the toxicity of anti-PD-1 and CTLA-4 immunotherapy. Cancer Cell 42:780–796. https://doi.org/10.1016/j.ccell.2024.03.001
30. Imodoye SO, Adedokun KA (2023) EMT-induced immune evasion: connecting the dots from mechanisms to therapy. Clin Exp Med. 23:4265–4287. https://doi.org/10.1007/s10238-023-01229-4
31. Jiang Y, Zhan H (2020) Communication between EMT and PD-L1 signaling: new insights into tumor immune evasion. Cancer Lett. 468:72–81. https://doi.org/10.1016/j.canlet.2019.10.013
32. Taki M et al (2021) Tumor immune microenvironment during epithelial-mesenchymal transition. Clin Cancer Res. 27:4669–4679. https://doi.org/10.1158/1078-0432.CCR-20-4459
33. Brest P, Mograbi B, Pages G, Hofman P, Milano G (2023) Checkpoint inhibitors and anti-angiogenic agents: a winning combination. Br J Cancer 129:1367–1372. https://doi.org/10.1038/s41416-023-02437-1
34. Rivera M, Bander ED, Cisse B (2021) Perspectives on microglia-based immune therapies against glioblastoma. World Neurosurg. 154:228–231. https://doi.org/10.1016/j.wneu.2021.06.127
35. Grabowski MM et al (2021) Immune suppression in gliomas. J Neurooncol. 151:3–12. https://doi.org/10.1007/s11060-020-03483-y
36. Yuan W et al (2023) Dual role of CXCL8 in maintaining the mesenchymal state of glioblastoma stem cells and M2-like tumor-associated macrophages. Clin Cancer Res. 29:3779–3792. https://doi.org/10.1158/1078-0432.CCR-22-3273
37. Chen S et al (2023) Macrophages in immunoregulation and therapeutics. Signal Transduct Target Ther. 8:207. https://doi.org/10.1038/s41392-023-01452-1